Calculations of impurity transport in Wendelstein 7-X plasmas

A. Mollén[1], M. Landreman[2], H. M. Smith[1], J. A. Alcusón[1], P. Xanthopoulos[1], J. M. García-Regaña[3], J. L. Velasco[3], A. Iantchenko[4], S. Buller[4], A. Langenberg[1], N. A. Pablant[5], P. Helander[1] and the W7-X Team

[1] *Max-Planck-Institut für Plasmaphysik, Greifswald, Germany*

[2] *Institute for Research in Electronics and Applied Physics, University of Maryland, USA*

[3] *Laboratorio Nacional de Fusión, CIEMAT, Madrid, Spain*

[4] *Department of Physics, Chalmers University of Technology, Göteborg, Sweden*

[5] *Princeton Plasma Physics Laboratory, Princeton, New Jersey, USA*

Introduction A major concern for the stellarator is the gradual accumulation of impurities in the center which is often observed in experiments, and which can lead to pulse termination by radiation collapse. Impurity transport is consequently a topic with significant attention. Collisional transport theory has traditionally predicted impurity accumulation in stellarators driven by the inward pointing radial electric field. However, recent advances in analytical [1, 2, 3] and numerical [4, 5, 6] studies suggest that the standard neoclassical theory lack several effects that can be crucial when analyzing the impurity transport, and perhaps the situation is less severe than previously thought. Here we study a Wendelstein 7-X (W7-X) plasma from the first experimental campaign and compare neoclassical impurity fluxes to experimental values.

SFINCS The SFINCS code (Stellarator Fokker-Planck Iterative Neoclassical Conservative Solver) is a continuum drift-kinetic solver and it is detailed in [5, 7]. The code solves the time-independent radially local 4D drift-kinetic equation for $f_{1s}(\theta,\zeta,x,\xi)$

$$\dot{\boldsymbol{R}}\cdot\nabla f_{1s}+\dot{v}_{\|}\frac{\partial f_{1s}}{\partial v_{\|}}-C_s=-f_{0s}\left[\frac{1}{n_{0s}}\frac{dn_{0s}}{dr}+\frac{Z_s e}{T_s}\frac{d\Phi_0}{dr}+\left(\frac{m_s v^2}{2T_s}-\frac{3}{2}+\frac{Z_s e}{T_s}\Phi_1\right)\frac{1}{T_s}\frac{dT_s}{dr}\right](\boldsymbol{v}_{\mathrm{d}s}+\boldsymbol{v}_{E1})\cdot\nabla r, \tag{1}$$

where the distribution function of species s is $f_s=f_{0s}+f_{1s}$, with $f_{1s}/f_{0s}\ll 1$, and

$$f_{0s}=f_{\mathrm{M}s}\exp\left(-Z_s e\Phi_1/T_s\right)=\frac{n_{0s}(r)}{\pi^{3/2}v_s^3}\exp\left[-\left(v_{\|}^2+v_{\perp}^2\right)/v_s^2-Z_s e\Phi_1/T_s\right]. \tag{2}$$

The particle trajectories are given by

$$\begin{aligned}
\dot{\boldsymbol{R}}&=v_{\|}\boldsymbol{b}+\frac{c}{B}(\boldsymbol{b}\times\nabla\Phi_0),\\
\dot{v}_{\|}&=-\frac{Z_s e}{m_s}\boldsymbol{b}\cdot\nabla\Phi_1-\mu\boldsymbol{b}\cdot\nabla B-\frac{cv_{\|}}{B^2}(\boldsymbol{b}\times\nabla B)\cdot\nabla\Phi_0,\\
\dot{\mu}&=0,
\end{aligned} \tag{3}$$

and we have defined the radial magnetic drift $\boldsymbol{v}_{ds}\cdot\nabla r = \frac{m_s c}{Z_s e B^2}\left(v_\perp^2/2 + v_\parallel^2\right)\boldsymbol{b}\times\nabla B\cdot\nabla r$ and the radial $\boldsymbol{E}\times\boldsymbol{B}$-drift velocity $\boldsymbol{v}_{E1} = (c/B)\,\boldsymbol{b}\times\nabla\Phi_1$ (the additional notation used herein is standard). Apart from f_{1s}, Eq. (1) contains the electrostatic potential on the flux-surface $\Phi_1(\theta,\zeta) = \Phi - \Phi_0(r)$, where $\Phi_0(r) = \langle\Phi\rangle$ and $|\Phi_1| \ll |\Phi_0|$ (the $\langle\ldots\rangle$ denotes a flux-surface average). SFINCS calculates the unknowns (f_{1s},Φ_1) by solving the coupled nonlinear system given by Eq. (1), the quasi-neutrality equation

$$\sum_s Z_s \int d^3v\, f_s = 0 \tag{4}$$

and

$$\langle\Phi_1\rangle = 0, \tag{5}$$

iteratively using Newton's method. Some features of the code are that it allows for an arbitrary number of kinetic species (including non-adiabatic electrons), can self-consistently calculate the ambipolar radial electric field $E_r = -d\Phi_0/dr$, and employs the linearized Fokker-Planck collision operator $C_{ab}^l \equiv C_{ab}[f_{1a}, f_{0b}] + C_{ab}[f_{0a}, f_{1b}]$.

Experimental discharge We use SFINCS to perform neoclassical calculations on a W7-X plasma from the first experimental campaign OP1.1, magnetic configuration J with central electron density $n_e = 0.14\times10^{20}$ m^{-3} and central temperatures $T_e = 4.6$ keV, $T_i = T_z = 1.1$ keV. Of particular interest are the radial particle fluxes of a tracer Ar^{16+}-impurity, where the calculations can be compared to experimental values inferred from XICS (X-ray Imaging Crystal Spectrometer) measurements [8, 9]. In Fig. 1 the plasma collisionalities are plotted, showing that the Ar^{16+}-impurities are collisional whereas the main species are at low collisionality.

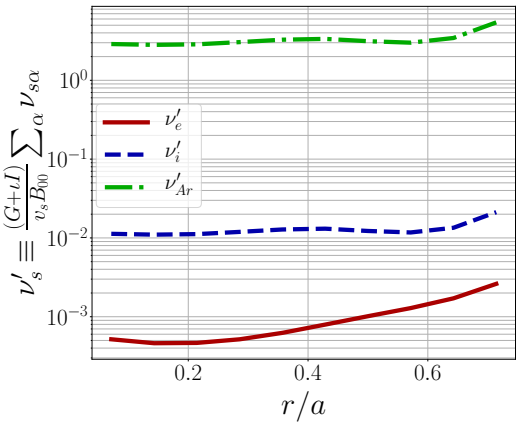

Figure 1: *Radial profiles of collisionalities of the electrons, main* H^+*-ions and tracer* Ar^{16+}*-impurities in the studied plasma.*

Figure 2 shows the radial profile of E_r calculated by SFINCS (neglecting Φ_1 for simplicity), the DKES (Drift Kinetic Equation Solver) code [10] and values from XICS measurements. The SFINCS calculations throughout this work use a minimum of $N_\theta = 25$, $N_\zeta = 165$ grid points in the poloidal and toroidal direction (per identical segment of the stellarator), $N_x = 8$ grid points in energy, $N_\xi = 274$ Legendre polynomials to represent the distribution function and $N_L = 4$ Legendre polynomials to represent the Rosenbluth potentials. The two codes conform well with each other, whereas there is a discrep-

ancy to the experimental values particularly in predicting where the transition from electron root ($E_r > 0$) to ion root ($E_r < 0$) happens in the plasma. This discrepancy could be related to profile evolution and often the agreement is better between codes and measurements [9].

Figure 3 shows a comparison between the normalized radial Ar^{16+}-flux, neglecting and including Φ_1 in the SFINCS calculations (the values neglecting Φ_1 agree well with results from the EUTERPE code [4]). We see that towards the plasma edge Φ_1 has a larger impact on the fluxes. In the figure the electrostatic potential is also illustrated on the central flux-surface $r/a = 0.5$ and given as a function of Boozer angular coordinates. The variation on the flux-surface is approximately ± 15 V which is similar to the variations predicted in other work for W7-X [5], but an order of magnitude smaller than calculations have found in some plasmas in the Large Helical Device. We note that for the radial $\boldsymbol{E} \times \boldsymbol{B}$-drift to be able to compete with the radial magnetic drift, and to modify the radial particle fluxes (compare the $\boldsymbol{v}_{E1}$ and the $\boldsymbol{v}_{ds}$ terms on the right-hand side of Eq. (1)), the ratio $Ze\Phi_1/T$ should be order unity. For Ar^{16+} in the studied plasma $Z_{Ar}e\Phi_1/T_{Ar} \sim 0.25$. SFINCS also implements an extension to Eq. (1) and can include a model of tangential magnetic drifts on the left-hand side [11]. However, incorporating this extra term in our calculations has a small impact on the Ar^{16+}-fluxes for the studied plasma.

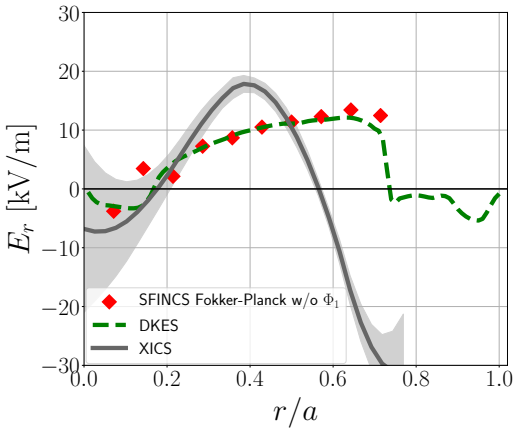

Figure 2: *Radial electric field calculated by* SFINCS, DKES *and inferred from XICS measurements.*

Finally, in Fig. 4 we show a comparison of radial Ar^{16+}-fluxes calculated by SFINCS and values inferred from XICS measurements (here we show values from calculations neglecting Φ_1, but the difference in the figure is small for calculations including Φ_1). Although the direction of the SFINCS values is the same as in the measurements (outward fluxes), it is clear that we are not able to reproduce the experimental transport levels with our neoclassical calculations. Particularly towards the plasma edge the discrepancy is large.

Discussion and conclusions Since our neoclassical calculations are not able to reproduce the experimental Ar^{16+}-fluxes throughout the plasma, it seems necessary to look for other transport channels. The classical flux is often neglected as smaller than the neoclassical flux, but in [12] it is shown that for a collisional impurity species classical transport can play a role. This is particularly the case for W7-X which has been optimized to have a low ratio of parallel to perpendicular current. However, for the studied plasma we find that the classi-

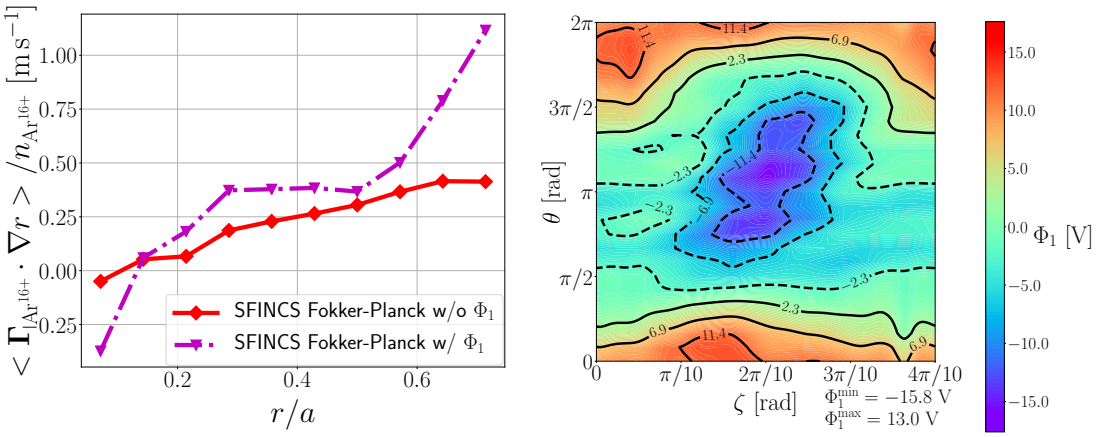

Figure 3: SFINCS *calculations of the neoclassical radial* Ar^{16+}*-flux neglecting and including* Φ_1 *(left).* $\Phi_1(\theta,\zeta)$ *on the flux-surface at* $r/a = 0.5$ *(right).*

cal Ar^{16+}-fluxes are generally less than 10 % of the neoclassical fluxes. To look at the turbulent transport is a natural candidate for explaining the discrepancy, but gyrokinetic simulations are extremely expensive for stellarator plasmas and not yet done on a routinely basis. Nevertheless, linear gyrokinetic simulations with the GENE code [13] indicate that for the studied plasma the linear growth rate of the most unstable mode increase rapidly towards the plasma edge, which is a step in the right direction.

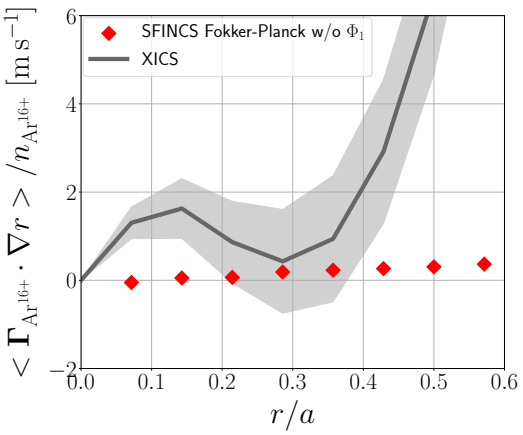

Figure 4: *The neoclassical radial* Ar^{16+}*-flux from* SFINCS *calculations (neglecting* Φ_1*) and values inferred from XICS measurements.*

[1] P. Helander, et al., *Phys. Rev. Lett.* **118** (2017) 155002.

[2] I. Calvo, et al., *Plasma Phys. Control. Fusion* **59** (2017) 055014.

[3] I. Calvo, et al., *arXiv:1803.05691* (2018).

[4] J. M. García-Regaña, et al., *Nucl. Fusion* **57** (2017) 056004.

[5] A. Mollén, et al., *Plasma Phys. Control. Fusion* **60** (2018) 084001.

[6] J. L. Velasco, et al., *Plasma Phys. Control. Fusion* **60** (2018) 074004.

[7] M. Landreman, et al., *Phys. Plasmas* **21** (2014) 042503.

[8] A. Langenberg, et al., *Nucl. Fusion* **57** (2017) 086013.

[9] N. A. Pablant, et al., *Phys. Plasmas* **25** (2018) 022508.

[10] S. P. Hirshman, et al., *Phys. Fluids* **29** (1986) 2951.

[11] E. J. Paul, et al., *Nucl. Fusion* **57** (2017) 116044.

[12] S. Buller, et al., *arXiv:1805.00972* (2018).

[13] F. Jenko, et al., *Phys. Plasmas* **7** (2000) 1904.

This work has been carried out within the framework of the EUROfusion Consortium and has received funding from the Euratom research and training programme 2014-2018 under grant agreement No 633053. The views and opinions expressed herein do not necessarily reflect those of the European Commission.